Macromolecules

pubs.acs.org/Macromolecules Article

Synthesis of Polyimides Containing Benzimidazole Groups in Side Chains for Natural Gas Separation

Xiaohua Tong, Guangran Shao, Ming Yuan, Xuewei Li, and Wangqing Zhang*

Cite This: *Macromolecules* 2024, 57, 11785−11795 Read Online

ACCESS | Metrics & More | Article Recommendations | Supporting Information

ABSTRACT: Polyimides for natural gas separation are synthesized from copolycondensation of 5-(1*H*-benzimidazol-2-yl)benzene-1,3-diamine (BIB) with 2,3,5,6-tetramethyl-1,4-phenylenediamine (Durene) and 4,4′-(hexafluoroisopropylidene)diphthalic anhydride (6FDA) with different 6FDA/BIB/Durene ratios. All polyimides containing benzimidazole groups in side chains display good processability, outstanding thermal stability, and excellent mechanical properties. The CO_2 permeability and CO_2/CH_4 selectivity of the synthesized polyimides change with the 6FDA/BIB/Durene ratio or the BIB content. At a total pressure of 2 bar and a CO_2/CH_4 feed ratio of 50:50, the polyimide synthesized with 30% BIB content ($F_{10}B_3D_7$) exhibits a high CO_2 permeability of 197.2 Barrer coupled with a high CO_2/CH_4 selectivity of 38.6, which is close to the 2008 Robeson's upper bound. Besides, CO_2-induced plasticization and physical aging of polyimide membranes can also be regulated by tuning the 6FDA/BIB/Durene ratio. Specifically, $F_{10}B_3D_7$ also exhibits good plasticization resistance and excellent stability against physical aging, and it is demonstrated to be a promising candidate for the purification of biogas and the removal of CO_2 molecules from natural gas.

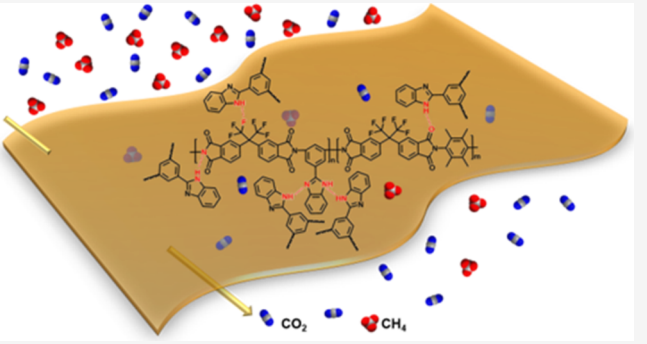

INTRODUCTION

With the continuous growth of the global population over the past 20 years, worldwide consumption of energy has expanded rapidly.[1−3] Natural gas provides significant support to meet increasing worldwide demand for energy due to its high thermal efficiency,[2,4] low carbon footprint, and clean combustion.[5−7] Unfortunately, raw natural gas contains a significant fraction of impurities such as carbon dioxide (CO_2), nitrogen (N_2), water vapor, and other undesirable gases, which should be removed before being delivered to the pipeline.[1,8−10] Among these gases, the acid gas CO_2 is the main contaminant, since it tends to induce corrosion of transport pipelines and processing equipment.[11−13] Currently, CO_2 capture technology using amines dominates acid gas treatment operations to meet the pipeline requirement (i.e., the concentration of CO_2 in natural gas must be less than 2%).[14−16] However, the absorption-based process is energy-intensive and brings environmental concerns besides high operating costs.[17,18] Membrane-mediated gas separation is one of the most promising alternative technologies,[19,20] owing to its small footprint, high energy efficiency, and low cost.[21,22] For large-scale industrial applications, gas separation membranes should have a high permeability coefficient to improve the efficiency of gas transport,[4,23] as well as high gas selectivity in order to gain the high-purity product.[24−26] However, the gas separation performance of polymer membranes is typically limited to an inherent trade-off effect between gas permeability and selectivity, first revealed by Robeson and later theoretically demonstrated by Freeman;[27] that is, membranes with high gas permeability show low selectivity for a specified gas pair and vice versa.[28,29]

In recent years, a number of materials have been exploited as gas separation membranes, such as cellulose acetates,[30] polyimides,[31,32] polysulfones,[33,34] carbon molecular sieves,[35−40] zeolites,[41] and so on. Among them, carbon molecular sieve membranes in hollow fiber formats exhibit excellent gas separation properties due to their unique pore structures, while their preparation processes still require an additional pyrolysis step, and their mechanical properties are poor. Aromatic polyimides, especially those based on 4,4′-(hexafluoroisopropylidene)diphthalic anhydride (6FDA), are among the most promising polymers because of their superior mechanical property and outstanding thermal and chemical stability.[42−44] However, 6FDA-based polyimides suffer from low permeability and moderate gas selectivity, which limits their large-scale application in gas separation. For example,

Received: October 2, 2024
Revised: November 22, 2024
Accepted: November 25, 2024
Published: December 5, 2024

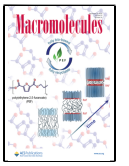

https://doi.org/10.1021/acs.macromol.4c02421
Macromolecules 2024, 57, 11785−11795

commercially available polyimide Matrimid 5218 has a low CO_2 permeability of 10 Barrer and a pure gas CO_2/CH_4 selectivity of 30.[44] The polyimide 6FDA-CF3BP prepared by de la Campa et al. had a low CO_2 permeability of 25 Barrer and a pure gas CO_2/CH_4 selectivity of 30.5.[45] It has been recently demonstrated that the gas permeability could be enhanced by incorporating bulky substituent groups and a contorted structure in the polyimide backbone to loosen the chain packing and increase the free volume.[31,46−48] Following this strategy, Huang and Chen et al. reported the synthesis of a series of microporous polyimides containing pendant bulky tetra-o-isopropyl substituents and rigid naphthalene units.[31] The resulting polyimide PI-3F exhibited excellent gas separation performance with a CO_2 permeability coefficient of 845 Barrer and a CO_2/CH_4 permselectivity of 15.4. Additionally, Freeman's theoretical analysis suggests that increasing the rigidity of the polyimide system is an effective way to increase CO_2/CH_4 selectivity.[49] Moreover, the CO_2/CH_4 selectivity can be tailored by incorporating polar substituent groups into the polyimide backbone.[1,2,50] For instance, Pinnau's group developed the TDA1-APAF polyimide derived from 9,10-dimethyl-2,3,6,7-triptycene tetracarboxylic dianhydride (TDA1) and diamine 2,2-bis(3-amino-4-hydroxyphenyl)-hexafluoropropane (APAF) with a high CO_2/CH_4 selectivity of 55 coupled with a moderate CO_2 permeability of 40 Barrer.[2] Despite this attractive recent progress, it remains a significant challenge to prepare polyimides with the optimal balance between permeability and selectivity.

According to a previous study,[51] the presence of 2,3,5,6-tetramethyl-phenyl moieties (Durene) in the polyimide backbone can loosen interchain packing to increase fractional free volume. Meanwhile, incorporating rigid benzimidazole groups is expected to increase the rigidity of the polymer backbone, modulate polymer chain spacing, and enhance interaction with CO_2 to improve CO_2 selectivity. In this work, a diamine containing a rigid benzimidazole group, 5-(1*H*-benzimidazol-2-yl)benzene-1,3-diamine (BIB), was initially synthesized, and then polyimides with different 6FDA/BIB/Durene ratios were synthesized by a polycondensation reaction of diamines (BIB and Durene) with 4,4′-(9-fluorenylidene)-dianiline (6FDA). Their corresponding CO_2 and CH_4 separation properties were investigated under pure, mixed, and humidified gas feed. Furthermore, the effect of the 6FDA/BIB/Durene ratio on the physical properties of polyimides, such as fractional free volume (FFV), glass transition temperature (T_g), water contact angle, and gas sorption, was studied in detail to understand the polymer structure−property relationship.

EXPERIMENTAL SECTION

Materials. 3,5-Dinitrobenzoic acid (Innochem, China), thionyl chloride ($SOCl_2$, Tianjin Bohua Reagent Co., Ltd.), *N*,*N*-dimethylformamide (DMF, Tianjin Bohua Reagent Co., Ltd.), *N*,*N*-dimethylacetamide (DMAc, Tianjin Bohua Reagent Co., Ltd.), *o*-phenylenediamine (Aladdin), phosphorus pentoxide (P_2O_5, Tianjin Bohua Reagent Co., Ltd.), methanesulfonic acid (CH_3SO_3H, Meryer), 80% hydrazine hydrate ($N_2H_4{\cdot}H_2O$, Tianjin Bohua Reagent Co., Ltd.), 5% Pd/C (Heowns), pyridine (Tianjin Bohua Reagent Co., Ltd.), acetic anhydride (Tianjin Bohua Reagent Co., Ltd.), tetrahydrofuran (THF, Tianjin Bohua Reagent Co., Ltd.), superdry *N*-methyl-2-pyrrolidone (superdry NMP, Tianjin Bohua Reagent Co., Ltd.), and 4,4′-(hexafluoroisopropylidene)diphthalic anhydride (6FDA, Innochem) were used as received. 2,3,5,6-Tetramethyl-1,4-phenylenediamine (Durene, Heowns) was purified by recrystallization from ethanol.

Synthesis of Monomers. *Synthesis of 3,5-Dinitrobenzoyl Chloride (i).* A mixture of 3,5-dinitrobenzoic acid (21.21 g, 10.0 mmol), $SOCl_2$ (47.58 g, 40.0 mmol), and the catalyst DMF (0.07 g, 1.0 mmol) was stirred at 78 °C for 6 h. Then, the reaction mixture was cooled to ambient temperature, and excess $SOCl_2$ was removed using distillation under vacuum. After drying in a vacuum oven at 40 °C for 10 h, 3,5-dinitrobenzoyl chloride (i) was obtained as a light yellow solid powder. Yield: 21.90 g, 95%. ^{1}H NMR (400 MHz, $CDCl_3$): δ 9.40 (t, J = 2.1 Hz, 1H), 9.30 (d, J = 2.2 Hz, 2H). Fourier-transform infrared (FT-IR) (cm^{-1}): 1761 (C═O stretching), 1534, 1338 (−NO_2 stretching).

Synthesis of 2-(3,5-Dinitrophenyl)-1H-benzimidazole (ii). To a dry 250 mL three-neck round-bottom flask, P_2O_5 (10 g) and CH_3SO_3H (100 g) were added under an argon atmosphere. The reaction mixture was stirred at room temperature for 24 h to form a clear and transparent solution, and after that, 3,5-dinitrobenzoyl chloride (5.41 g, 50.0 mmol) and *o*-phenylenediamine (11.53 g, 50.0 mmol) were added. The reaction system was heated to 120 °C and kept there for 15 h. After cooling to ambient temperature, the reaction solution was poured into deionized water, and the precipitate was collected via filtration under reduced pressure. The crude product was further recrystallized from DMF, later washed with ethanol, and dried to obtain the final product as a yellow powder. Yield: 9.06 g, 73%. ^{1}H NMR (400 MHz, DMSO-d_6): δ 13.57 (s, 1H), 9.32 (d, J = 2.1 Hz, 2H), 8.83 (d, J = 2.3 Hz, 1H), 7.68 (s, 2H), 7.30 (dt, J = 6.2, 3.5 Hz, 2H). FT-IR (cm^{-1}): 3329 (N−H stretching), 1526, 1346 (−NO_2 stretching).

Synthesis of 5-(1H-Benzimidazol-2-yl)benzene-1,3-diamine (iii, BIB). 2-(3,5-Dinitrophenyl)-1*H*-benzimidazole (8.53 g, 30.0 mmol) and Pd/C (0.09 g) were added to 120 mL of ethanol. The suspension was heated to 78 °C for 0.5 h, and thereafter, $N_2H_4{\cdot}H_2O$ (6.01 g, 120.0 mmol) was added dropwise. The reaction mixture was refluxed for 10 h, cooled to ambient temperature, and poured into deionized water. The formed precipitate was then filtrated, washed with acetone three times, and dried under vacuum at 60 °C for 5 h. The crude product was finally recrystallized from ethanol and dried at 80 °C for 8 h to yield the desired diamine monomer as a white powder. Yield: 5.72 g, 85%. ^{1}H NMR (400 MHz, DMSO-d_6): δ 12.52 (s, 1H), 7.61−7.53 (m, 1H), 7.49−7.41 (m, 1H), 7.15 (dd, J = 7.5, 4.5 Hz, 1H), 7.13 (d, J = 2.9 Hz, 1H), 6.61 (d, J = 1.9 Hz, 2H), 5.96 (d, J = 2.0 Hz, 1H), 4.93 (s, 4H). FT-IR (cm^{-1}): 3320 (N−H stretching), 3395, 3225 (−NH_2 stretching).

Synthesis of Polyimides. Six 6FDA-based polyimides were prepared via a conventional two-stage polymerization reaction and named $F_{10}B_xD_{1-x}$ based on the molar ratio of 6FDA, BIB, and Durene of $10/x/10-x$.

This general preparation process is shown by an example of $F_{10}B_5D_5$. Under an argon atmosphere, BIB (0.45 g, 2.0 mmol) and Durene (0.33 g, 2.0 mmol) were dissolved in superdry NMP (5.8 mL). After that, 6FDA (1.78 g, 4.0 mmol) was added to this solution. After stirring for 12 h, the mixture of pyridine (0.16 g, 2.0 mmol) and acetic anhydride (0.41 g, 4.0 mmol) was added dropwise. Then, the reaction temperature was raised to 120 °C and maintained for 10 h. After cooling, the viscous solution was poured into deionized water, filtered, and washed repeatedly with water and ethanol. The precipitate was dried in a vacuum oven at 80 °C for 10 h to give the final polymer as a white solid.

$F_{10}B_{10}$: ^{1}H NMR (400 MHz, DMSO-d_6): δ 13.18 (s, 1H), 8.39 (s, 1H), 8.23 (s, 2H), 8.01 (s, 3H), 7.79 (d, J = 33.9 Hz, 3H), 7.61 (s, 2H), 7.22 (s, 2H). FT-IR (cm^{-1}): 1787 (C═O asymmetric stretching), 1723 (C═O symmetric stretching), 1348 (C−N stretching), and 850 (imide ring deformation).

$F_{10}B_8D_2$: ^{1}H NMR (400 MHz, DMSO-d_6): δ 13.20 (s, 0.8H), 8.39 (s, 0.8H), 8.24 (d, J = 8.3 Hz, 2H), 7.96 (d, J = 34.8 Hz, 3.2H), 7.82 (d, J = 12.3 Hz, 1.6H), 7.75 (dd, J = 3.6, 1.8 Hz, 0.8H), 7.61 (s, 1.6H), 7.23 (s, 1.6H), 2.07 (s, 2.4H). FT-IR (cm^{-1}): 1782 (C═O asymmetric stretching), 1719 (C═O symmetric stretching), 1348 (C−N stretching), and 845 (imide ring deformation).

https://doi.org/10.1021/acs.macromol.4c02421
Macromolecules 2024, 57, 11785−11795

$F_{10}B_5D_5$: ^{1}H NMR (400 MHz, DMSO-d_6): δ 13.17 (s, 0.5H), 8.39 (s, 0.5H), 8.22 (d, J = 9.2 Hz, 2H), 7.92 (dt, J = 35.8, 19.2 Hz, 4.5H), 7.75 (d, J = 2.3 Hz, 0.5H), 7.61 (d, J = 34.9 Hz, 1H), 7.22 (s, 1H), 2.07 (s, 6H). FT-IR (cm^{-1}): 1787 (C═O asymmetric stretching), 1719 (C═O symmetric stretching), 1352 (C−N stretching), and 850 (imide ring deformation).

$F_{10}B_3D_7$: ^{1}H NMR (400 MHz, DMSO-d_6): δ 13.17 (s, 0.3H), 8.39 (s, 0.3H), 8.30−8.13 (m, 2H), 7.95 (q, J = 20.5, 16.9 Hz, 4.3H), 7.75 (s, 0.3H), 7.62 (s, 0.6H), 7.22 (s, 0.6H), 2.07 (s, 8.4H). FT-IR (cm^{-1}): 1782 (C═O asymmetric stretching), 1719 (C═O symmetric stretching), 1353 (C−N stretching), 855 (imide ring deformation).

$F_{10}B_1D_9$: ^{1}H NMR (400 MHz, DMSO-d_6): δ 13.18 (s, 0.1H), 8.39 (s, 0.1H), 8.21 (d, J = 8.1 Hz, 2H), 7.98 (d, J = 7.3 Hz, 4H), 7.75 (s, 0.2H), 7.62 (s, 0.2H), 7.23 (s, 0.2H), 2.08 (s, 10.8H). FT-IR (cm^{-1}): 1787 (C═O asymmetric stretching), 1719 (C═O symmetric stretching), 1348 (C−N stretching), and 850 (imide ring deformation).

$F_{10}D_{10}$: ^{1}H NMR (400 MHz, DMSO-d_6): δ 8.22 (d, J = 7.7 Hz, 2H), 7.98 (s, 4H), 2.08 (s, 12H). FT-IR (cm^{-1}): 1787 (C═O asymmetric stretching), 1723 (C═O symmetric stretching), 1352 (C−N stretching), 855 (imide ring deformation).

Membrane Preparation. The polyimides were dissolved in DMAc (10% w/v) to form transparent polymer solutions and then purified by using 0.2 μm polytetrafluoroethylene filters. Thereafter, the solutions were poured onto leveled glasses, and the solvent was slowly evaporated at 60 °C for 72 h. The obtained polyimide membranes were further dried in a vacuum oven at 130 °C for 30 h. To remove the residual solvent, dry polyimide membranes (∼60 to 80 μm) were soaked in an ethanol/THF mixture (90/10 by volume) for 15 h and then dried in a vacuum oven at 80 °C for 24 h.

Characterization. The characterization details can be found in the Supporting Information.

Gas Permeation Testing. The pure gas permeability coefficients of CO_2 and CH_4 were determined at 1 bar via a constant-pressure/variable-volume method. The mixed gas (CO_2/CH_4 = 50/50 by volume) permeation properties of the polyimide membranes were measured at 2 bar under dry and humidified conditions, respectively. Moreover, the polyimide membranes were measured at CO_2 partial pressures of 0.5, 1, 2, 3, 4, 5, and 6 bar under dry conditions. The gas permeation apparatus is shown in Figure S1. The gas permeability coefficient was calculated using eq 1

$$P_i = \frac{Q_i l}{\Delta P_i A} \tag{1}$$

where P_i refers to the permeability coefficient (Barrer), Q_i refers to the volumetric flow rate of gas component i (cm^3/s (STP)), l refers to the membrane thickness (cm), ΔP_i refers to the transmembrane pressure difference (cmHg), and A refers to the effective area of the polyimide membrane (cm^2). The ideal selectivity (α) for a given gas pair (i and j) is determined by eq 2

$$\alpha_{i/j} = \frac{P_i}{P_j} \tag{2}$$

RESULTS AND DISCUSSION

The diamine monomer BIB was synthesized from commercially available 3,5-dinitrobenzoic acid via a three-step protocol, as shown in Scheme 1. In the first step, 3,5-dinitrobenzoic acid was reacted with $SOCl_2$ using DMF as a catalyst to form 3,5-dinitrobenzoyl chloride (i). In the next step, intermediate (i) was converted to the dinitro compound (ii) by the reaction with 1,2-benzenediamine in the presence of P_2O_5 and CH_3SO_3H. Lastly, intermediate (ii) was reduced using $N_2H_4{\cdot}H_2O$ and Pd/C to afford the desired diamine monomer BIB (iii). The structures of all compounds (i−iii) were confirmed by FT-IR and ^{1}H NMR (Figures S2−S5).

Scheme 1. Synthesis of the Diamine Monomer BIB

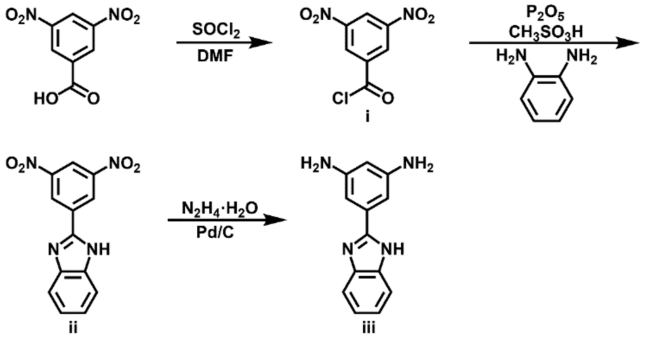

All polyimides were synthesized by a conventional two-step polycondensation reaction in superdry NMP with a catalytic amount of acetic anhydride and pyridine at 120 °C, as shown in Scheme 2. The chemical structures of the polyimides were fully characterized by FT-IR and ^{1}H NMR spectroscopy (Figures S6 and S7). The characteristic imide absorption bands appear at approximately 1790 cm^{-1} (C═O asymmetric stretching), 1720 cm^{-1} (C═O symmetric stretching), 1350 cm^{-1} (C−N stretching), and 850 cm^{-1} (imide ring deformation), confirming the successful preparation of the polyimides. Figure S7 shows the ^{1}H NMR spectra of the polyimides, in which each proton of polyimides could be unambiguously distributed according to the integral values of the intensity. The absorption bands at the 7.0−9.0 ppm region are assigned to aromatic protons, while the protons of methyl groups appear at 2.55 ppm. The peak at 13 ppm represents the proton of the benzimidazole substituent group. Meanwhile, no signal peak corresponding to the proton of the carboxylic acid group is observed at about 10 ppm, further confirming complete imidization of the polyimides. All polymers display high number average molecular weights in the range of 98−136 kg mol^{-1} and narrow polydispersity indexes of 1.65−1.79, as determined by GPC using DMF as eluent (Table S1 and Figure S8).

It is well known that traditional aromatic polyimides own limited solubility in most organic solvents, which astricts their applications in the field of gas separation.[47,52] However, six polyimides prepared in this work were readily soluble in many aprotic solvents and protic solvents such as DMAc, THF, DMSO, etc. (Table S2). The reason is ascribed to the synergetic effects of the substituent groups among pendant benzimidazole, methyl, and trifluoromethyl, which destroy the regularity of polymer chains and inhibit the close chain packing, consequently permitting organic solvents to dissolve the polyimides more easily. The good solubility of the present polyimides is useful for the preparation of self-standing membranes for gas separation.

By first casting polyimide solution in DMF at 60 °C and then drying the membranes to remove solvent, polyimide membranes were obtained. It is found that when the laser passes through the polyimide membranes, no scattering is observed (Figure S9), confirming that these membranes are homogeneous. Moreover, high transmittance in the transmittance spectrum and the absence of an obvious scattering peak in small-angle X-ray scattering (SAXS) patterns of polyimide membranes further confirm that the polyimide membranes are homogeneous without significant microphase separation (Figure S9).

https://doi.org/10.1021/acs.macromol.4c02421
Macromolecules 2024, 57, 11785−11795

Scheme 2. Synthesis of 6FDA-Based Polyimides

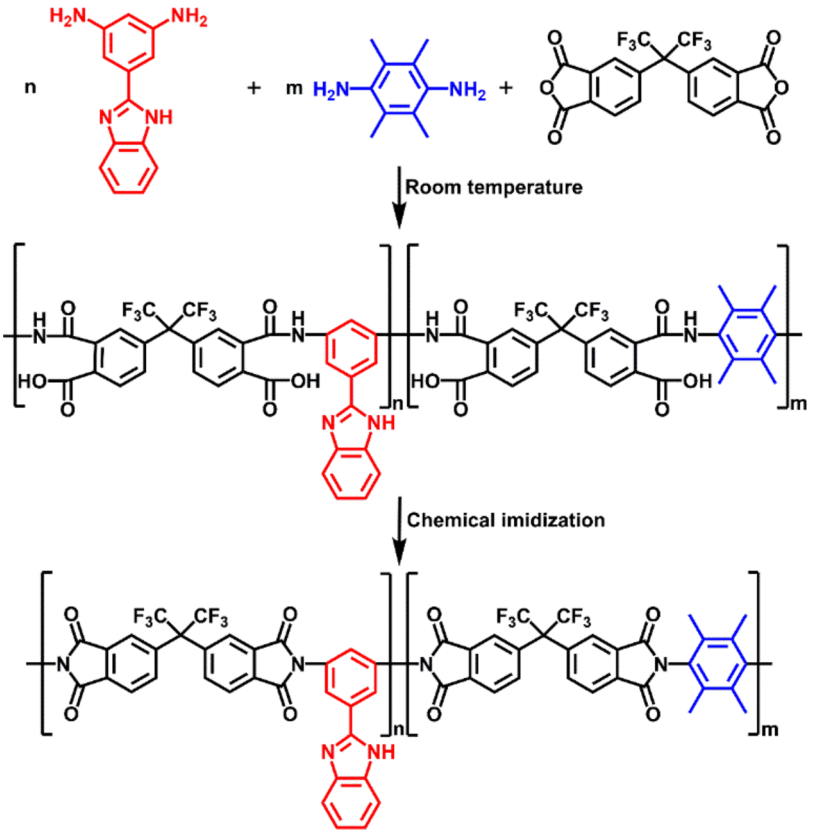

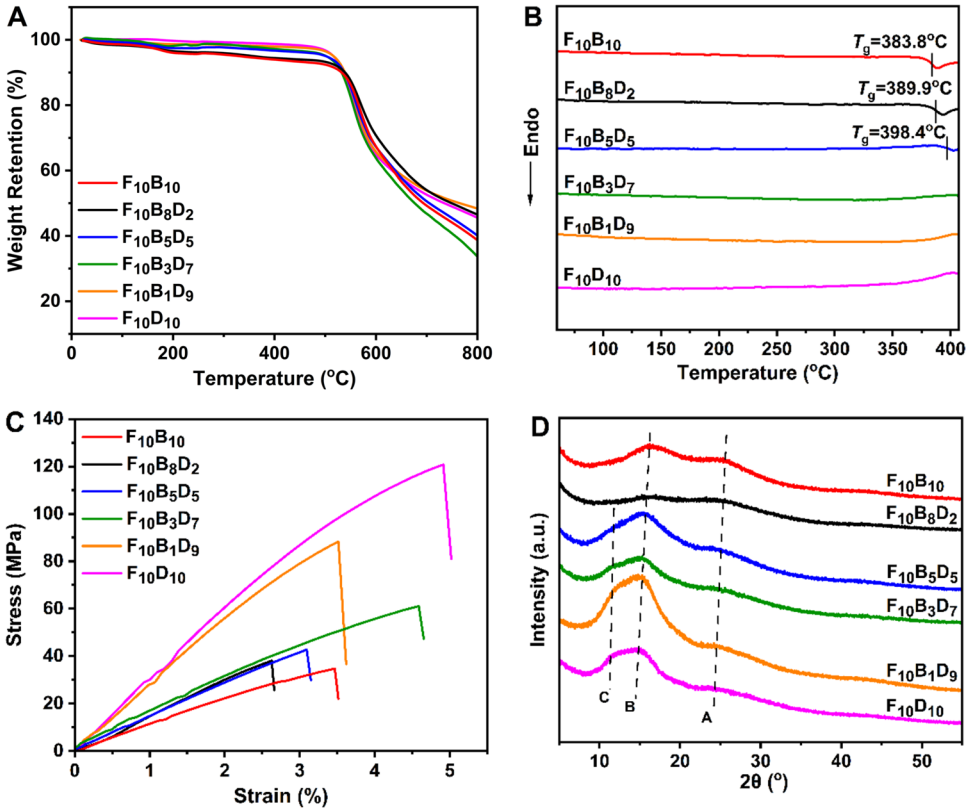

Figure 1. TGA curves of 6FDA-based polyimides (A), DSC curves of 6FDA-based polyimides (B), stress−strain curves of 6FDA-based polyimides (C), and WAXD spectra of 6FDA-based polyimides (D).

https://doi.org/10.1021/acs.macromol.4c02421
Macromolecules 2024, 57, 11785−11795

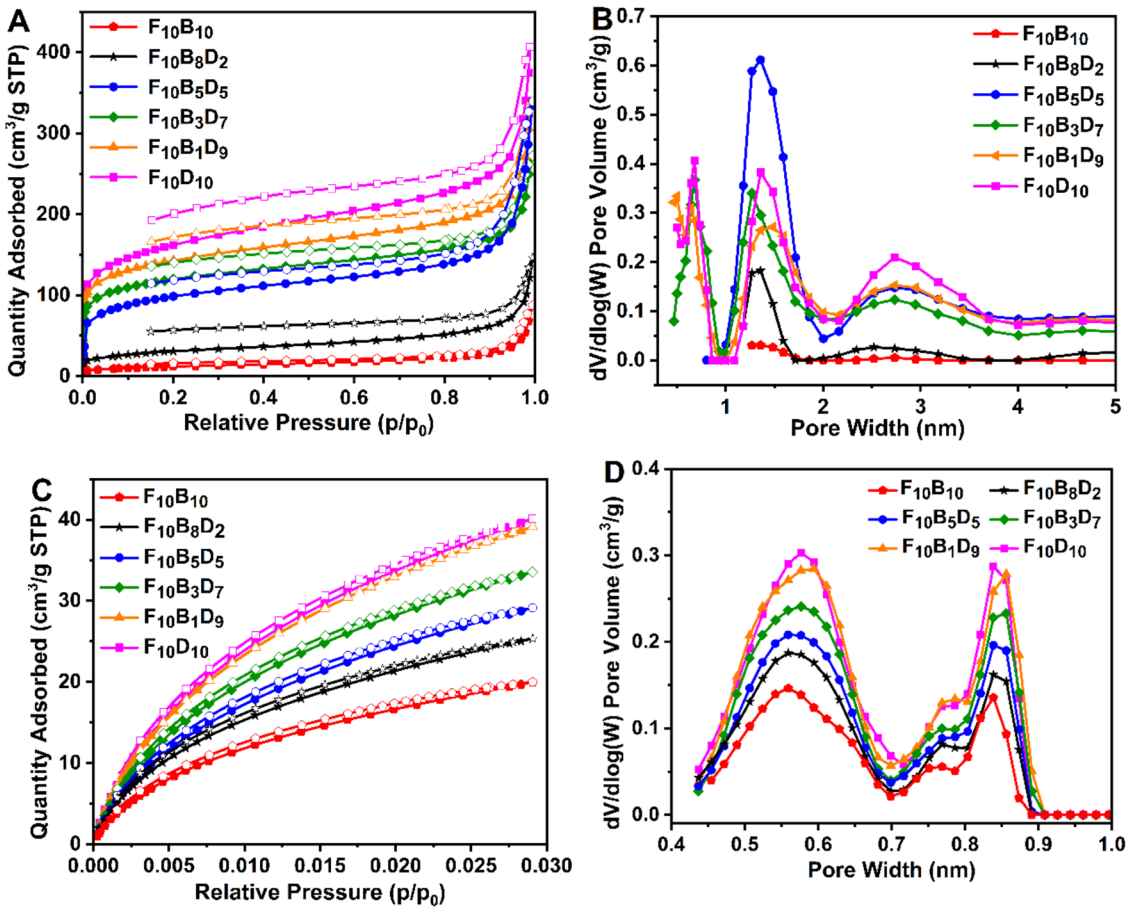

Figure 2. N_2 isotherms (A) and pore size distribution (B) of 6FDA-based polyimides measured at 77K (B), and CO_2 isotherms (C) and pore size distribution (D) of 6FDA-based polyimides measured at 273 K.

Thermal gravimetric analysis (TGA) was performed to assess the thermal properties of the polyimide membranes. As shown in Figure 1A, all polyimides gradually convey a small mass loss between 25 and 250 °C ascribed to adsorbed solvent or water. $F_{10}B_{10}$ and $F_{10}B_8D_2$ exhibit more mass loss up to 250 °C as compared to other polyimides, possibly due to the fact that they contain more benzimidazole groups and thus have a stronger ability to entrap high-boiling solvent and absorb moisture from air. In addition, derivative thermogravimetric (DTG) curves of all polyimides show two decomposition steps, which are typically observed for 6FDA-based polyimides (Figure S10). Mass loss in the region of 400−600 °C appears to be linked to the degradation of C−F bonds, imide rings, and benzimidazole groups. The second stage starts at ∼610 °C and is primarily associated with further carbonization of the polymer chains containing benzimidazole groups and 2,3,5,6-tetramethyl-phenyl moieties.

Glass transition temperatures (T_g) of six polyimides were evaluated by a differential scanning calorimeter (DSC). As shown in Figure 1B, $F_{10}B_{10}$ displays the lowest T_g value with 383.8 °C, which is due to the high rotational mobility of this 6FDA-based polyimide containing benzimidazole groups in side chains. $F_{10}B_8D_2$ possesses a higher T_g value than $F_{10}B_{10}$ because of the presence of methyl substituent groups in the 2,3,5,6-tetramethyl-phenyl moiety of Durene that restricts internal rotation of the polymer backbone. Moreover, the T_g value of copolyimides increases from 389.9 to 398.4 °C with the 6FDA/Durene/BIB ratio increasing from 10:8:2 to 10:5:5, suggesting an increase in the chain rigidity due to the introduction of more 2,3,5,6-tetramethyl-phenyl moieties of Durene into the main chain. For other polyimides in the series, no glass transition temperature was detected up to 410 °C. The result confirms that the chain rigidity of the polyimides can be finely regulated by controlling the 6FDA/BIB/Durene ratio in the polyimide backbone.

As shown in Figure 1C, the polyimide membranes exhibit tensile strengths in the range of 30−120 MPa with elongation at break values of 2.6−4.9%, suggesting that they own excellent mechanical properties for permeability testing. The good mechanical properties are due to the strong intermolecular interaction force.

As shown in Figure S11, the water contact angles of all polymer membranes are lower than 90°, suggesting their somewhat hydrophilic nature. The water contact angle increases in the following order: $F_{10}B_{10}$ < $F_{10}B_8D_2$ < $F_{10}B_5D_5$ < $F_{10}B_3D_7$ < $F_{10}B_1D_9$ < $F_{10}D_{10}$. That is to say, the higher the BIB content in the polymer, the smaller the water contact angle and the stronger the hydrophilicity. This results from the presence of benzimidazole groups in the BIB moiety. Through hydrogen bonding, the benzimidazole groups on the polymer backbone interact with the water molecule to form a hydration layer, which enhances the hydrophilicity of the membrane.

Wide-angle X-ray diffraction (WAXD) analysis of six polyimide membranes was conducted to elucidate the effect of distinct substituent groups, namely, benzimidazole groups and methyl groups, on the polymer chain packing. As shown in

https://doi.org/10.1021/acs.macromol.4c02421
Macromolecules 2024, 57, 11785−11795

Table 1. Physical Properties of 6FDA-Based Polyimides

polymer	S_{BET}[a] (m^2/g)	CO_2 uptake[b] (cm^3/g)	M[c] (g/mol)	ρ[d] (g/cm^3)	V[e]	V_w[f]	FFV[g]
$F_{10}B_{10}$	43	20.0	632	1.30	486.2	327.1	0.125
$F_{10}B_8D_2$	112	25.3	620	1.25	496.0	326.7	0.144
$F_{10}B_5D_5$	358	29.1	602	1.21	497.5	326.2	0.148
$F_{10}B_3D_7$	440	33.6	590	1.17	504.3	325.8	0.160
$F_{10}B_1D_9$	525	39.1	578	1.12	516.1	325.5	0.180
$F_{10}D_{10}$	591	40.1	572	1.09	524.8	325.3	0.194

[a]BET surface area determined by N_2 isotherms at 77 K. [b]CO_2 uptake determined by CO_2 isotherms at 273 K. [c]The molar mass of the polyimide repeat unit. [d]The density of the polyimide. [e]The molar volume of the polyimide ($V = M/\rho$). [f]The van der Waals volume of the polyimide. [g]Fractional free volume determined by the group contribution method.

Figure 1D and Table S3, all polyimide membranes display a broad scattering feature, confirming their amorphous nature. WAXD spectra of $F_{10}B_{10}$ and $F_{10}B_8D_2$ exhibit two peaks, which correspond to different interchain spacings. Peak B at around 5.5 Å (d_2) relates to the region of efficiently packed polymer molecular chains arising from the rigidity of the polymer backbone, while peak A located in the 3.5 Å range (d_1) is ascribed to $\pi-\pi$ stacking caused by aromatic rings. For the other four polyimides, additional peak C at ~7 Å (d_3) appears in the scattering pattern. The result indicates that bulky methyl groups in polyimides are able to separate adjacent polymer molecular chains more effectively than benzimidazole groups and lead to polyimides with larger *d*-spacings. In addition, it is worth noting that all *d*-spacing values corresponding to scattering peaks increase gradually with the increase of the content of 2,3,5,6-tetramethyl-phenyl moieties of Durene in polyimides. Specifically, an increase in the d_2 value from 5.45 Å in $F_{10}B_{10}$ to 6.06 Å in $F_{10}D_{10}$ is observed. Similarly, $F_{10}B_{10}$ shows the lowest d_1 value (3.56 Å), while $F_{10}D_{10}$ displays the highest d_1 value (3.74 Å) in the 6FDA-based polyimides. This increased *d*-spacing may be due to more disturbed polymer chain packing caused by a significant fraction of methyl substituent groups. The trend is consistent with the gas transport performance of the polyimides, as discussed below.

Microstructure analysis of all polyimides was carried out using gas adsorption. Nitrogen adsorption at −196 °C demonstrates that $F_{10}B_{10}$ has low microporosity, which could be ascribed to strong cohesive interactions between polyimide molecular chains owing to polar benzimidazole groups (Figure 2A,B). In contrast, nitrogen adsorption isotherms from other polyimides in the series all exhibit high gas uptake at low relative pressures indicative of the presence of a large number of micropores. The apparent BET surface areas of 6FDA-based polyimides range from 43 to 591 m^2/g and follow the order of $F_{10}B_{10}$ (43 m^2/g) < $F_{10}B_8D_2$ (112 m^2/g) < $F_{10}B_5D_5$ (358 m^2/g) < $F_{10}B_3D_7$ (440 m^2/g) < $F_{10}B_1D_9$ (525 m^2/g) < $F_{10}D_{10}$ (591 m^2/g). Hence, it can be concluded that the introduction of the Durene moiety into polyimide is significantly more efficient in inducing micropores than the introduction of the BIB moiety.

Gas sorption of CO_2 at 0 °C was also performed both to measure the CO_2 uptake and to evaluate the pore size distribution (PSD). As shown in Figure 2C, CO_2 uptakes are within the range of 20−40 cm^3/g, and the CO_2 adsorption isotherms of the polyimides agree with the overall trend displayed in N_2 adsorption isotherms. Pore size distribution calculated from CO_2 isotherms indicates micropores in the region of 4−9 Å (Figure 2D). As expected with the increase of BIB content, three primary peaks shift toward the region of smaller pore width, and pore volume decreases, which favors the enhancement of CO_2/CH_4 selectivity.

Fractional free volume (FFV) was also collected to further investigate the backbone structure of the polyimide (Table 1). 6FDA-based polyimides exhibit FFV values of 0.125−0.194, which are typical values for aromatic polyimides.[31,51] Consistent with the result determined by gas sorption, $F_{10}B_{10}$ displays the lowest FFV value of 0.122, owing to its strong interchain interaction, allowing for denser chain packing. The polyimides containing methyl substituent groups exhibit higher FFV values because of greater disruption of polyimide chain packing.

The pure gas permeabilities of CO_2 and CH_4 of the polyimide membranes were determined by the constant-pressure/variable-volume technique at 1 bar at 25 °C. The gas separation data for six polyimide membranes are summarized in Table 2. As shown in Table 2, with the increase in the relative content of the Durene moiety in the polymer main chain, the gas permeability of the polyimides increases monotonously, whereas the CO_2/CH_4 selectivity decreases. This trend qualitatively agrees with the result from FFV and BET surface areas discussed above. Specifically, $F_{10}B_{10}$ displays a moderate CO_2 permeability of 38.2 Barrer and a high CO_2/CH_4 selectivity of 38.2, possibly due to the strong interactions between benzimidazole groups and CO_2 molecules. Compared with $F_{10}B_{10}$, $F_{10}B_8D_2$ exhibits a significant increase in CO_2 permeability coefficient by almost 74% (66.5 Barrer vs 38.2 Barrer) with a slightly small drop in pure gas selectivity (35.0 vs 38.2). The result suggests that the incorporation of a low Durene content into the polymer chain hardly compromises the CO_2/CH_4 selectivity. In the case of $F_{10}B_3D_7$ with much higher Durene content, the polyimide $F_{10}B_3D_7$ shows an ~4.5-fold increase in the CO_2 permeability coefficient to 209.8 Barrer and ~16% loss in selectivity to 32.2 in comparison to $F_{10}B_{10}$, which is an excellent combination of high permeability and high selectivity. In the case of $F_{10}B_1D_9$ with further high Durene content, an improvement in permeability at the expense of CO_2/CH_4 selectivity is detected. It exhibits an enhanced CO_2 permeability coefficient of around 430 Barrer, whereas the CO_2/CH_4 selectivity decreases to 25.0. This can

Table 2. Pure Gas Permeability (P) and Selectivity (α) of 6FDA-Based Polyimides

polymer	P (CO_2)	P (CH_4)	α (CO_2/CH_4)
$F_{10}B_{10}$	38.2 ± 5.4	1.0 ± 0.2	38.2 ± 2.3
$F_{10}B_8D_2$	66.5 ± 3.3	1.9 ± 0.5	35.0 ± 2.8
$F_{10}B_5D_5$	135.0 ± 6.3	4.0 ± 0.2	33.7 ± 1.7
$F_{10}B_3D_7$	209.8 ± 13.8	6.5 ± 0.8	32.2 ± 2.4
$F_{10}B_1D_9$	431.3 ± 11.9	17.2 ± 0.5	25.0 ± 0.3
$F_{10}D_{10}$	519.6 ± 34.2	28.8 ± 1.4	18.0 ± 0.3

https://doi.org/10.1021/acs.macromol.4c02421
Macromolecules 2024, 57, 11785−11795

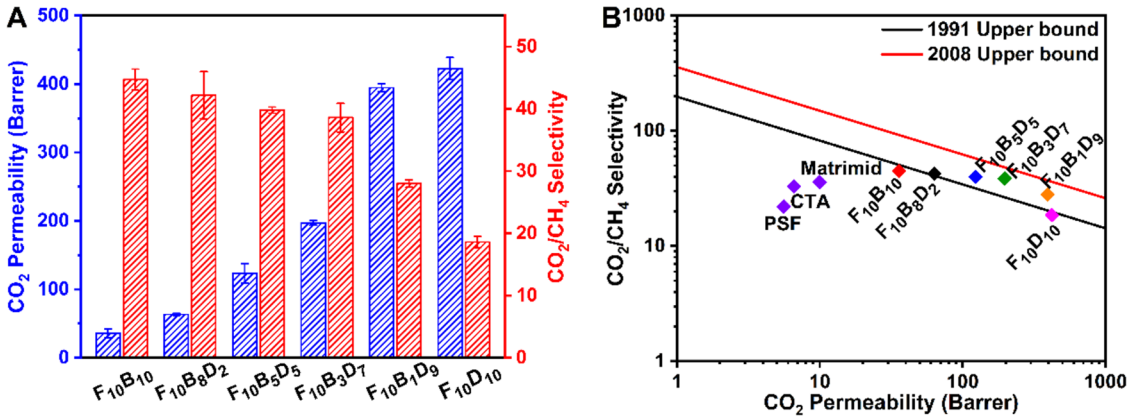

Figure 3. Mixed gas separation properties of 6FDA-based polyimides with different BIB/Durene ratios under the dry state (A), Robeson plots relevant to 6FDA-based polyimides with different BIB/Durene ratios (B).

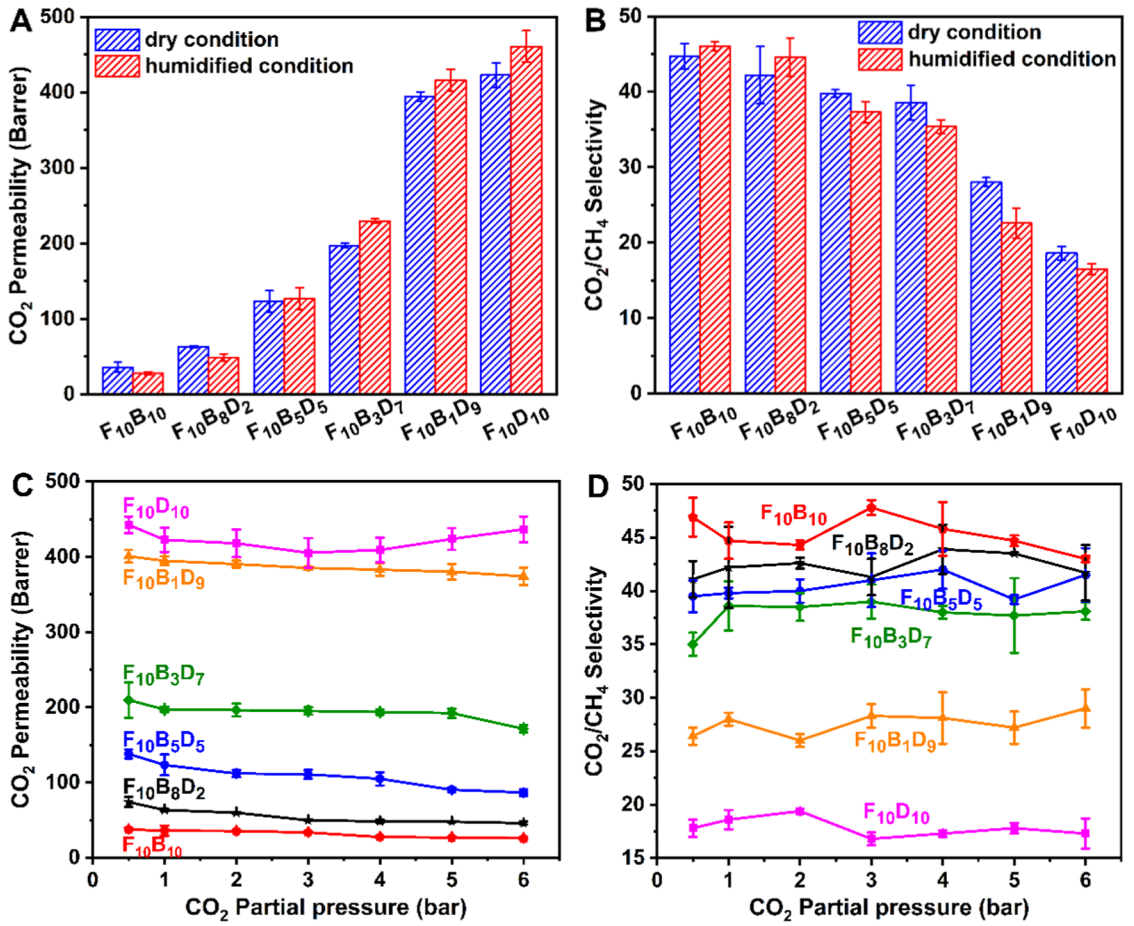

Figure 4. Mixed gas CO_2 permeability of 6FDA-based polyimides under the dry state and the humidified state (A), mixed gas CO_2/CH_4 selectivity of 6FDA-based polyimides under the dry state and the humidified state (B), mixed gas CO_2 permeability versus CO_2 partial pressure of 6FDA-based polyimides (C), and mixed gas CO_2/CH_4 selectivity versus CO_2 partial pressure of 6FDA-based polyimides (D).

be ascribed to loose polymer chain packing caused by the introduction of a large number of methyl groups in the polymer backbone. Therefore, it is concluded that the copolymerization of BIB and Durene is an effective way to improve the comprehensive separation performance of polyimide materials.

Although polyimide membranes show promising results under pure gas feed conditions, the investigation of mixed gas separation is more practical to evaluate their true performance.[53,54] Herein, the binary mixed gas separation performance of all polyimide membranes was checked at a 50:50 CO_2/CH_4 feed ratio and a total 2 bar pressure, as shown in Figures 3A and S12. The mixed gas separation properties of polyimide membranes differ from the corresponding pure gas permeation properties. Specifically, the mixed gas CO_2 and CH_4 permeabilities are both lower than those determined under a single-gas environment at the same partial pressure, most likely due to the competitive sorption effect, leading to increased

https://doi.org/10.1021/acs.macromol.4c02421
Macromolecules 2024, 57, 11785−11795

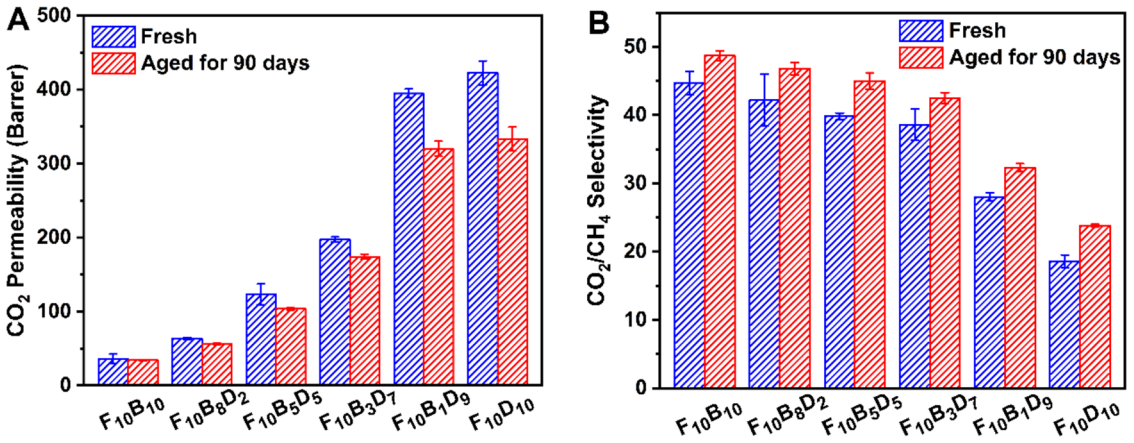

Figure 5. Fresh and aged mixed gas CO_2 permeability of 6FDA-based polyimides (A), fresh and aged mixed gas CO_2/CH_4 selectivity of 6FDA-based polyimides (B).

CO_2/CH_4 permselectivity. Moreover, the decrease in CO_2 permeability is less dramatic, which can be attributed to the high affinity between the CO_2 gas and sorption sites in the polymer matrix. For example, $F_{10}B_3D_7$ displays mixed gas permeability at 197.2 Barrer for CO_2 and 5.1 Barrer for CH_4 with the CO_2/CH_4 permselectivity at 38.6, in which the CO_2 permeability is about 6.0% lower than the pure CO_2 permeability, the CH_4 permeability is about 21.5% lower than the pure CH_4 permeability, and the CO_2/CH_4 permselectivity is about 19.9% higher than the calculated value of 32.2 based on pure gas permeability. Similarity was reported previously,[28,55] and this is ascribed to CO_2 preferentially occupying the sorption sites of polyimide membranes by strong sorption interaction and therefore hindering the transport of CH_4 in gas mixtures.

As is well known, one of the most authoritative approaches for accessing the potential of novel polymer materials for the separation of given gas pairs is to place their data on Robeson diagrams to evaluate their position relative to the empirical upper bound.[56] The CO_2/CH_4 Robeson plot for the six polyimides is shown in Figure 3B. CO_2/CH_4 separation data for three commercially available gas separation membranes, i.e., polysulfone (PSF),[33,34] polyimide (Matrimid 5218),[44] and cellulose triacetate (CTA),[30] are also included in Figure 3B for comparison. As shown in Figure 3B, $F_{10}B_{10}$ and $F_{10}B_8D_2$ display low CO_2 permeability, resulting in the positions of their data falling below the 1991 Robeson upper bound. The data of $F_{10}D_{10}$ are also located below the upper bound, which is due to its poor selectivity. The data from $F_{10}B_5D_5$, $F_{10}B_3D_7$, and $F_{10}B_1D_9$ lie between the published 1991 and 2008 CO_2/CH_4 upper bounds, and $F_{10}B_3D_7$ lies very close to the 2008 upper bound, suggesting that it has the most excellent overall properties in terms of the permeability/permselectivity trade-off effect for CO_2/CH_4 separation. In addition, it is important to note that $F_{10}B_3D_7$ exhibits both a higher permeability coefficient and higher permselectivity for CO_2/CH_4 gas pairs than PSF, e.g., the permeability coefficient of CO_2 increases ~34-fold from 10 to 197.2 Barrer, and the selectivity is improved from 22 to 38.6. $F_{10}B_3D_7$ has a similar CO_2/CH_4 selectivity to that of Matrimid 5218 but has an over 1 order higher permeability. These results indicate that the $F_{10}B_3D_7$ polyimide prepared in this work is very promising for natural gas and biogas purification.

To evaluate the effect of water on gas permeation through polyimide membranes, the permeability coefficients of CO_2 and CH_4 under the humidified condition were measured, and the results are summarized in Figures 4A,B and S13. For $F_{10}B_{10}$ and $F_{10}B_8D_2$, the humidified CO_2 permeability coefficient is lower than the value acquired under the dry state, whereas the CO_2/CH_4 selectivity is higher. The drop in the CO_2 permeability can likely be ascribed to the following two reasons. First, water molecules can fill the voids among polyimide chains and therefore reduce the gas transport channels. Second, the interaction of water with the benzimidazole groups, imide groups, and trifluoromethyl groups leads to a hydrated layer on the membrane surface, which obstructs gas diffusion. Instead, in the case of polyimide with high Durene content, polyimide membranes are more permeable to CO_2 and CH_4 under the humidified state combined with reduced CO_2/CH_4 selectivity compared to dry polyimide membranes. For example, when the dried $F_{10}B_3D_7$ membrane becomes humidified, the CO_2 permeability coefficient increases from 197.2 to 229.8 Barrer, while the CO_2/CH_4 selectivity decreases from 38.6 to 35.4. The unique gas transport properties exhibited by four polyimides ($F_{10}B_5D_5$, $F_{10}B_3D_7$, $F_{10}B_1D_9$, and $F_{10}D_{10}$) under the humidified state are attributed to two factors. On the one hand, water causes polymer membranes to swell, and as a result, polymer chain packing becomes less compact and more free volume elements in polyimides are generated, which has been observed in previously reported literature studies.[57−59] On the other hand, water is able to react with CO_2 to generate HCO_3^-, which promotes CO_2 permeation by lowering the energy barrier.

A major challenge affecting the large-scale application of polymer gas separation membrane materials is plasticization, where condensable gas molecules such as CO_2 can cause the polymer membranes to swell, inducing increased chain mobility as well as weakened molecular-sieving properties, thus drastically reducing permselectivity.[46,60] Herein, high-pressure mixed gas permeation measures were performed in order to investigate the plasticization of the polymer membranes prepared in this work. As seen in Figures 4C and S14, the plasticization pressure of $F_{10}D_{10}$ is as low as 4 bar. This value is relatively low probably because of bulky methyl substituent groups, which weaken the interchain forces and make segmental mobility increase. In comparison, no plasticization pressure point is detected when $F_{10}B_{10}$ is

https://doi.org/10.1021/acs.macromol.4c02421
Macromolecules 2024, 57, 11785−11795

subjected to a CO_2 partial feed pressure of up to approximately 6 bar in the mixed gas case, demonstrating outstanding resistance to penetrant-induced plasticization. This is mainly due to tighter interchain packing resulting from strong hydrogen-bonded interchain interactions. Similar results are detected for other polyimides, which realize a drop in CO_2 permeability when the CO_2 partial pressure is increased from 0.5 to 6.0 bar. For instance, for $F_{10}B_3D_7$, its CO_2 permeability falls from 209.7 Barrer to 171.5 Barrer as CO_2 partial pressure goes from 0.5 to 6 bar. Moreover, the CO_2/CH_4 selectivity remains relatively stable over the entire CO_2 partial feed pressure range for all of the polyimides (Figure 4D). This confirms that the benzimidazole group is an excellent building block for helping prevent polymer matrix swelling induced by CO_2 molecules. However, future work is needed to evaluate the gas separation performance of polyimide membranes under more aggressive feed conditions, i.e., partial pressures of CO_2 up to 30−40 bar, in order to fully demonstrate their potential for application in state-of-the-art natural gas separation processes.

Physical aging is another important challenge for gas separation polymer membrane materials in terms of the potential to transition from laboratory to industry application.[5] Traditionally, aging leads to densification of the glassy polymer toward its equilibrium packing state and thus loss in gas permeability accompanied by improvement in permselectivity. Figures 5 and S15 summarize the corresponding data of permeability and permselectivity of all samples prepared in this work after aging for 90 days at room temperature. Relative to the fresh $F_{10}D_{10}$ membrane, the aged $F_{10}D_{10}$ membrane follows the tendency commonly observed in previously reported 6FDA-based polyimides,[5] producing a 21% decrease in CO_2 permeability (422.6 Barrer vs 333.1 Barrer) combined with a slight increase in CO_2/CH_4 selectivity (18.6 vs 23.8). This is ascribed to the fact that part of the conformational free volume collapses over time, influencing gas transport. For $F_{10}B_1D_9$, the decrease in CO_2 permeability is less, with only a 19% drop from 394.7 to 320.0 Barrer after aging for 90 days. In addition, it is worth noting that the other four polyimides containing the BIB moiety exhibit excellent stability against aging, in which CO_2/CH_4 selectivity remains essentially unchanged and CO_2 permeabilities decrease less than 16% over 90 days. This can be rationalized as a tightening of polymer chain packing caused by the presence of the benzimidazole group, inhibiting the movement of molecular chains.

CONCLUSIONS

In summary, a series of polyimides were synthesized by polymerization of 6FDA with BIB and Durene with different monomer ratios. The resulting polyimides display high molecular weights, excellent solution-processability, and good mechanical properties, making them suitable for forming self-standing membranes for gas separation. Mixed gas permeation results suggest that tuning the 6FDA/BIB/Durene ratio in the polyimide main chain displays a different effect on permeability and selectivity. Increasing the 6FDA/BIB/Durene ratio results in higher CO_2/CH_4 selectivity with a decrease in permeability, whereas increasing Durene content in polyimide leads to an increase in permeability. The good balance between high gas permeability and high CO_2/CH_4 selectivity makes $F_{10}B_3D_7$ a competitive membrane material with separation performance located very near the 2008 upper bound for the CO_2/CH_4 gas pair. Moreover, CO_2-induced plasticization and physical aging of polyimide membranes can also be regulated by tuning the 6FDA/BIB/Durene ratio. Specifically, $F_{10}B_3D_7$ exhibits good plasticization resistance and excellent stability against physical aging. Taking into consideration the global quest for sustainable and clean energy, the preparation of such a membrane with superior gas separation properties opens a door to natural gas upgrading.

ASSOCIATED CONTENT

Supporting Information

The Supporting Information is available free of charge at https://pubs.acs.org/doi/10.1021/acs.macromol.4c02421.

Additional experimental data including schematic diagram of gas permeation apparatus; ^{1}H NMR spectra of the intermediates (i and ii) and monomer BIB; FT-IR spectra of the intermediates (i and ii) and monomer BIB; FT-IR spectra of 6FDA-based polyimides; ^{1}H NMR spectra of 6FDA-based polyimides; GPC traces of 6FDA-based polyimides; photos of 6FDA-based polyimides; photos of $F_{10}B_{10}$ and glass through laser light; photos of $F_{10}B_{10}$ and polyethylene (PE) through laser light; SAXS patterns of 6FDA-based polyimides; transmittance spectrum of 6FDA-based polyimides; derivative thermogravimetric curves of 6FDA-based polyimides; water contact angles of 6FDA-based polyimides; mixed gas CH_4 permeability of 6FDA-based polyimides under the dry state; mixed gas CH_4 permeability of 6FDA-based polyimides under the dry state and the humidified state; mixed gas CH_4 permeability versus CO_2 partial pressure of 6FDA-based polyimides; fresh and aged mixed gas CO_2 permeability of 6FDA-based polyimides; molecular weight and polydispersity index of 6FDA-based polyimides; solubility of 6FDA-based polyimides; and 2θ and d-spacing values of 6FDA-based polyimides (PDF)

AUTHOR INFORMATION

Corresponding Author

Wangqing Zhang − *Key Laboratory of Functional Polymer Materials of the Ministry of Education, Institute of Polymer Chemistry, College of Chemistry, Nankai University, Tianjin 300071, China; Frontiers Science Center for New Organic Matter and Tianjin Key Laboratory of Functional Polymer Materials, Nankai University, Tianjin 300071, China;* orcid.org/0000-0003-2005-6856; Phone: 86-22-23509794; Email: wqzhang@nankai.edu.cn; Fax: 86-22-23503510

Authors

Xiaohua Tong − *Key Laboratory of Functional Polymer Materials of the Ministry of Education, Institute of Polymer Chemistry, College of Chemistry, Nankai University, Tianjin 300071, China*

Guangran Shao − *Key Laboratory of Functional Polymer Materials of the Ministry of Education, Institute of Polymer Chemistry, College of Chemistry, Nankai University, Tianjin 300071, China*

Ming Yuan − *Key Laboratory of Functional Polymer Materials of the Ministry of Education, Institute of Polymer Chemistry, College of Chemistry, Nankai University, Tianjin 300071, China*

Xuewei Li − *Key Laboratory of Functional Polymer Materials of the Ministry of Education, Institute of Polymer Chemistry, College of Chemistry, Nankai University, Tianjin 300071, China*

Complete contact information is available at: https://pubs.acs.org/10.1021/acs.macromol.4c02421

Notes

The authors declare no competing financial interest.

■ ACKNOWLEDGMENTS

The financial support by the Ministry of Science and Technology of the People's Republic of China (2022YFB3804600) and the National Natural Science Foundation of China (No. 21931003) is gratefully acknowledged.

■ REFERENCES

(1) Yi, S.; Ma, X.; Pinnau, I.; Koros, W. J. A high-performance hydroxyl-functionalized polymer of intrinsic microporosity for an environmentally attractive membrane-based approach to decontamination of sour natural gas. *J. Mater. Chem. A* **2015**, *3* (45), 22794−22806.

(2) Alghunaimi, F.; Ghanem, B.; Alaslai, N.; Mukaddam, M.; Pinnau, I. Triptycene dimethyl-bridgehead dianhydride-based intrinsically microporous hydroxyl-functionalized polyimide for natural gas upgrading. *J. Membr. Sci.* **2016**, *520*, 240−246.

(3) Uc-Fernández, E.; Sulub-Sulub, R.; González-Díaz, A.; Herrera-Kao, W.; Ávila-Ortega, A.; Cetina-Mancilla, E.; Aguilar-Vega, M. J.; González-Díaz, M. O. Semi-biobased polyamide membranes derived from 2,5-furandicarboxylic acid for gas separation. *ACS Sustainable Chem. Eng.* **2024**, *12* (27), 10152−10163.

(4) Zhu, L.; Tian, D.; Shin, D.; Jia, W.; Bae, C.; Lin, H. Effects of tertiary amines and quaternary ammonium halides in polysulfone on membrane gas separation properties. *J. Polym. Sci., Part B:Polym. Phys.* **2018**, *56* (18), 1239−1250.

(5) Low, Z.-X.; Budd, P. M.; McKeown, N. B.; Patterson, D. A. Gas permeation properties, physical aging, and its mitigation in high free volume glassy polymers. *Chem. Rev.* **2018**, *118* (12), 5871−5911.

(6) Alaslai, N.; Ma, X.; Ghanem, B.; Wang, Y.; Alghunaimi, F.; Pinnau, I. Synthesis and characterization of a novel microporous dihydroxyl-functionalized triptycene-diamine-based polyimide for natural gas membrane separation. *Macromol. Rapid Commun.* **2017**, *38* (18), No. 1700303.

(7) Torres, D.; Pérez-Rodríguez, S.; Cesari, L.; Castel, C.; Favre, E.; Fierro, V.; Celzard, A. Review on the preparation of carbon membranes derived from phenolic resins for gas separation: From petrochemical precursors to bioresources. *Carbon* **2021**, *183*, 12−33.

(8) Yi, S.; Ghanem, B.; Liu, Y.; Pinnau, I.; Koros, W. J. Ultraselective glassy polymer membranes with unprecedented performance for energy-efficient sour gas separation. *Sci. Adv.* **2019**, *5* (5), No. eaaw5459.

(9) Elashkar, A. H.; Hedley, G. S.; Qazvini, O. T.; Telfer, S. G.; Cowan, M. G. An upper bound visualization of design trade-offs in adsorbent materials for gas separations: alkene/alkane adsorbents. *Chem. Commun.* **2021**, *57* (57), 6950−6959.

(10) Ma, Y.-Y.; Liu, M.; Wang, J.-T.; Zhu, B.; Li, Y.-F. Enhanced gas separation performance by embedding submicron poly(ethylene glycol) capsules into polyetherimide membrane. *Chin. J. Polym. Sci.* **2021**, *39* (3), 355−364.

(11) Meckler, S. M.; Bachman, J. E.; Robertson, B. P.; Zhu, C.; Long, J. R.; Helms, B. A. Thermally rearranged polymer membranes containing tröger's base units have exceptional performance for air separations. *Angew. Chem., Int. Ed.* **2018**, *57* (18), 4912−4916.

(12) Wang, C.; Chen, X.; Yao, S.; Peng, F.; Xiong, L.; Guo, H.; Zhang, H.; Chen, X. Effect of different oxygen-containing groups on the nanopore diameter of hyper-crosslinked resins for gas adsorption/separation. *ACS Appl. Nano Mater.* **2024**, *7* (1), 415−423.

(13) Murali, R. S.; Jha, A.; Aarti; Divekar, S.; Dasgupta, S. Synthesis and characterization of a high-performance bio-based Pebax membrane for gas separation applications. *Mater. Adv.* **2023**, *4* (20), 4843−4851.

(14) Radmanesh, F.; Elshof, M. G.; Benes, N. E. Polyoctahedral silsesquioxane hexachlorocyclotriphosphazene membranes for hot gas separation. *ACS Appl. Mater. Interfaces* **2021**, *13* (7), 8960−8966.

(15) Robinson, A. M.; Xia, Y. Regioisomeric Spirobifluorene CANAL ladder polymers and their gas separation performance. *ACS Macro Lett.* **2024**, *13* (2), 118−123.

(16) Zhang, Q.; Zheng, J.; Zhang, B.; Linga, P. Coal mine gas separation of methane via clathrate hydrate process aided by tetrahydrofuran and amino acids. *Appl. Energy* **2021**, *287*, No. 116576.

(17) Rodriguez, K. M.; Lin, S.; Wu, A. X.; Han, G.; Teesdale, J. J.; Doherty, C. M.; Smith, Z. P. Leveraging free volume manipulation to improve the membrane separation performance of amine-functionalized PIM-1. *Angew. Chem., Int. Ed.* **2021**, *60* (12), 6593−6599.

(18) Bahrami, A.; Raisi, A. Polyurethane-based blend membrane containing polycarbonate for gas separation: compatibility analysis, microstructure evaluation, and CO_2 separation performance. *Ind. Eng. Chem. Res.* **2024**, *63* (2), 1080−1099.

(19) Abdulhamid, M. A.; Lai, H. W. H.; Wang, Y.; Jin, Z.; Teo, Y. C.; Ma, X.; Pinnau, I.; Xia, Y. Microporous polyimides from ladder diamines synthesized by facile catalytic arene-norbornene annulation as high-performance membranes for gas separation. *Chem. Mater.* **2019**, *31* (5), 1767−1774.

(20) Zhang, B.; Li, J.; Zhang, L.; Wu, D. Tuning free volume for enhanced gas separation by introducing fluorinated aryl ether diamine moiety in Tröger's-based membranes. *Int. J. Hydrogen Energy* **2024**, *62*, 749−759.

(21) Chen, X.; Fan, Y.; Wu, L.; Zhang, L.; Guan, D.; Ma, C.; Li, N. Ultra-selective molecular-sieving gas separation membranes enabled by multi-covalent-crosslinking of microporous polymer blends. *Nat. Commun.* **2021**, *12*, No. 6140.

(22) Hu, X.; Mu, H.; Miao, J.; Lu, Y.; Wang, X.; Meng, X.; Wang, Z.; Yan, J. Synthesis and gas separation performance of intrinsically microporous polyimides derived from sterically hindered binaphthalenetetracarboxylic dianhydride. *Polym. Chem.* **2020**, *11* (25), 4172−4179.

(23) Abdulhamid, M. A.; Ma, X.; Miao, X.; Pinnau, I. Synthesis and characterization of a microporous 6FDA-polyimide made from a novel carbocyclic pseudo Tröger's base diamine: Effect of bicyclic bridge on gas transport properties. *Polymer* **2017**, *130*, 182−190.

(24) Ghanem, B. S.; Swaidan, R.; Ma, X.; Litwiller, E.; Pinnau, I. Energy-efficient hydrogen separation by AB-type ladder-polymer molecular sieves. *Adv. Mater.* **2014**, *26* (39), 6696−6700.

(25) Cheng, X.; Chen, B.; Zhao, G.; Tang, G.; Qin, P.; Liu, Y.; Li, P. Effects of ortho functional groups on the thermo-oxidative cross-linking process and gas separation properties of phenolphthalein-based polyimides. *Macromolecules* **2024**, *57* (10), 5050−5062.

(26) Yang, L.; Yang, H.; Wu, H.; Zhang, L.; Ma, H.; Liu, Y.; Wu, Y.; Ren, Y.; Wu, X.; Jiang, Z. COF membranes with uniform and exchangeable facilitated transport carriers for efficient carbon capture. *J. Mater. Chem. A* **2021**, *9* (21), 12636−12643.

(27) Ma, X.; Mukaddam, M.; Pinnau, I. Bifunctionalized intrinsically microporous polyimides with simultaneously enhanced gas permeability and selectivity. *Macromol. Rapid Commun.* **2016**, *37* (11), 900−904.

(28) Wang, Y.; Kumar, V.; Elahi, F.; Ghanem, B.; Balcik, M.; Shen, J.; Han, Y.; Pinnau, I. Amidoxime-functionalized tetraphenylethylene ladder polymer for efficient membrane-based gas separations. *Eur. Polym. J.* **2024**, *209*, No. 112896.

(29) Zhu, Z.; Dong, H.; Li, K.; Li, Q.; Li, J.; Ma, X. One-step synthesis of hydroxyl-functionalized fully carbon main chain PIMs via a Friedel-Crafts reaction for efficient gas separation. *Sep. Purif. Technol.* **2021**, *262*, No. 118313.

(30) Schell, W. J.; Wensley, C. G.; Chen, M. S. K.; Venugopal, K. G.; Miller, B. D.; Stuart, J. A. Recent advances in cellulosic membranes for gas separation and pervaporation. *Gas Sep. Purif.* **1989**, *3* (4), 162−169.
(31) Li, T.; Liu, J.; Zhao, S.; Chen, Z.; Huang, H.; Guo, R.; Chen, Y. Microporous polyimides containing bulky tetra-o-isopropyl and naphthalene groups for gas separation membranes. *J. Membr. Sci.* **2019**, *585*, 282−288.
(32) Wang, S.; Ma, S.; He, H.; Ai, W.; Wang, D.; Zhao, X.; Chen, C. Aromatic polyimides containing pyridine and spirocyclic units: Preparation, thermal and gas separation properties. *Polymer* **2019**, *168*, 199−208.
(33) McHattie, J. S.; Koros, W. J.; Paul, D. R. Gas transport properties of polysulphones: 1. Role of symmetry of methyl group placement on bisphenol rings. *Polymer* **1991**, *32* (5), 840−850.
(34) Saqib, S.; Rafiq, S.; Muhammad, N.; Khan, A. L.; Mukhtar, A.; Ullah, S.; Nawaz, M. H.; Jamil, F.; Zhang, C.; Ashokkumar, V. Sustainable mixed matrix membranes containing porphyrin and polysulfone polymer for acid gas separations. *J. Hazard. Mater.* **2021**, *411*, No. 125155.
(35) Lei, L.; Pan, F.; Lindbråthen, A.; Zhang, X.; Hillestad, M.; Nie, Y.; Bai, L.; He, X.; Guiver, M. D. Carbon hollow fiber membranes for a molecular sieve with precise-cutoff ultramicropores for superior hydrogen separation. *Nat. Commun.* **2021**, *12* (1), No. 268.
(36) Zhang, C.; Koros, W. J. Ultraselective carbon molecular sieve membranes with tailored synergistic sorption selective properties. *Adv. Mater.* **2017**, *29* (33), No. 1701631.
(37) Iyer, G. M.; Ku, C.; Zhang, C. Polyamide-imide copolymer-derived carbon molecular sieve membranes for efficient hydrogen/carbon dioxide separation. *Carbon* **2024**, *216*, No. 118598.
(38) Cao, Y.; Zhang, K.; Sanyal, O.; Koros, W. J. Carbon molecular sieve membrane preparation by economical coating and pyrolysis of porous polymer hollow fibers. *Angew. Chem., Int. Ed.* **2019**, *58* (35), 12149−12153.
(39) Wang, K.; Fang, C.; Li, Z.; Zhao, G.; Wang, Y.; Song, Z.; Lei, L.; Xu, Z. Oxygen-enriched carbon molecular sieve hollow fiber membrane for efficient CO_2 removal from natural gas. *Sep. Purif. Technol.* **2024**, *347*, No. 127611.
(40) He, X.; Chu, Y.; Lindbråthen, A.; Hillestad, M.; Hägg, M. Carbon molecular sieve membranes for biogas upgrading: Techno-economic feasibility analysis. *J. Cleaner Prod.* **2018**, *194*, 584−593.
(41) Rangnekar, N.; Mittal, N.; Elyassi, B.; Caro, J.; Tsapatsis, M. Zeolite membranes - a review and comparison with MOFs. *Chem. Soc. Rev.* **2015**, *44* (20), 7128−7154.
(42) Zhao, W.; Zhang, J.; Liu, C.; Ma, Y.; Li, K.; Guo, M.; Jiao, L.; Ma, X.; Yang, L.; Yang, S.; Cheng, B. Fine-tuning gas separation performance of intrinsic microporous polyimide by the regulation of atomic-level halogen substitution. *J. Membr. Sci.* **2024**, *692*, No. 122317.
(43) Wang, F.; Zhao, G.; Liu, Y.; Tang, G.; Qin, P.; Li, P. Development of phenolphthalein-based copolyimides and their derivative cross-linked and thermally rearranged polymers for gas separation. *Macromolecules* **2024**, *57* (3), 1370−1382.
(44) Sanders, D. F.; Smith, Z. P.; Guo, R.; Robeson, L. M.; McGrath, J. E.; Paul, D. R.; Freeman, B. D. Energy-efficient polymeric gas separation membranes for a sustainable future: A review. *Polymer* **2013**, *54* (18), 4729−4761.
(45) Álvarez, C.; Lozano, Á. E.; Juan-y-Seva, M.; de la Campa, J. G. Gas separation properties of aromatic polyimides with bulky groups. Comparison of experimental and simulated results. *J. Membr. Sci.* **2020**, *602*, No. 117959.
(46) Rodriguez, K. M.; Lin, S.; Wu, A. X.; Storme, K. R.; Joo, T.; Grosz, A. F.; Roy, N.; Syar, D.; Benedetti, F. M.; Smith, Z. P. Penetrant-induced plasticization in microporous polymer membranes. *Chem. Soc. Rev.* **2024**, *53* (5), 2435−2529.
(47) Wang, S.; Jin, S.; Han, X.; Li, L.; Zhao, X.; Zhou, H.; Chen, C. Insights into the relationship between structure and properties of spirobichroman-based polyimides: Effects of substituents on molecular structure and gas separation. *Mater. Des.* **2020**, *194*, No. 108933.
(48) Zhang, B.; Qiao, J.; Dong, C.; Yi, C.; Qi, S.; Yang, B. Dibenzo-21-crown-7-ether contained 6FDA-based polyimide membrane with improved gas selectivity. *Sep. Purif. Technol.* **2021**, *264*, No. 118454.
(49) Freeman, B. D. Basis of permeability/selectivity tradeoff relations in polymeric gas separation membranes. *Macromolecules* **1999**, *32* (2), 375−380.
(50) Liu, Z.; Liu, Y.; Qiu, W.; Koros, W. J. Molecularly engineered 6FDA-based polyimide membranes for sour natural gas separation. *Angew. Chem., Int. Ed.* **2020**, *59* (35), 14877−14883.
(51) Hayek, A.; Alsamah, A.; Shalabi, Y. A.; Saleem, Q.; Ben Sultan, M. M.; Alhajry, R. H. Molecular design of poly(imide-oxadiazole) membranes for high-pressure mixed-gas separation. *Macromolecules* **2022**, *55* (9), 3747−3761.
(52) Zhang, C.; Li, P.; Cao, B. Effects of the side groups of the spirobichroman-based diamines on the chain packing and gas separation properties of the polyimides. *J. Membr. Sci.* **2017**, *530*, 176−184.
(53) Lai, H. W. H.; Benedetti, F. M.; Ahn, J. M.; Robinson, A. M.; Wang, Y.; Pinnau, I.; Smith, Z. P.; Xia, Y. Hydrocarbon ladder polymers with ultrahigh permselectivity for membrane gas separations. *Science* **2022**, *375* (6587), 1390−1392.
(54) Huang, L.-J.; Weng, Y.-T.; Raiz, A.; Mao, Z.-J.; Ma, X.-H. Remarkably improved gas separation performance of polyimides by forming "bent and battered" main chain using paracyclophane as building block. *Chin. J. Polym. Sci.* **2023**, *41* (10), 1617−1628.
(55) Xiao, Y.; Lei, X.; Zhang, Z.; Chen, S.; Xiong, G.; Ma, X.; Zhang, Q. Carbazole-based polyimide membranes with hydrogen-bonding interactions for gas separation. *Macromolecules* **2024**, *57* (12), 5941−5957.
(56) Carta, M.; Malpass-Evans, R.; Croad, M.; Rogan, Y.; Jansen, J. C.; Bernardo, P.; Bazzarelli, F.; McKeown, N. B. An efficient polymer molecular sieve for membrane gas separations. *Science* **2013**, *339* (6117), 303−307.
(57) Xin, Q.; Li, Z.; Li, C.; Wang, S.; Jiang, Z.; Wu, H.; Zhang, Y.; Yang, J.; Cao, X. Enhancing the CO_2 separation performance of composite membranes by the incorporation of amino acid-functionalized graphene oxide. *J. Mater. Chem. A* **2015**, *3* (12), 6629−6641.
(58) Li, Y.; Xin, Q.; Wu, H.; Guo, R.; Tian, Z.; Liu, Y.; Wang, S.; He, G.; Pan, F.; Jiang, Z. Efficient CO_2 capture by humidified polymer electrolyte membranes with tunable water state. *Energy Environ. Sci.* **2014**, *7* (4), 1489−1499.
(59) Qu, Z.; Wu, H.; Zhou, Y.; Yang, L.; Wu, X.; Wu, Y.; Ren, Y.; Zhang, N.; Liu, Y.; Jiang, Z. Constructing interconnected ionic cluster network in polyelectrolyte membranes for enhanced CO_2 permeation. *Chem. Eng. Sci.* **2019**, *199*, 275−284.
(60) Corrado, T. J.; Huang, Z.; Huang, D.; Wamble, N.; Luo, T.; Guo, R. Pentiptycene-based ladder polymers with configurational free volume for enhanced gas separation performance and physical aging resistance. *Proc. Natl. Acad. Sci. U.S.A.* **2021**, *118* (37), No. e2022204118.